Applied Catalysis B: Environmental 232 (2018) 288–298

Contents lists available at ScienceDirect

Applied Catalysis B: Environmental

journal homepage: www.elsevier.com/locate/apcatb

Synergetic removal of Pb(II) and dibutyl phthalate mixed pollutants on Bi_2O_3-TiO_2 composite photocatalyst under visible light

Suzhen You[a], Yun Hu[a,b,c,*], Xingchen Liu[a], Chaohai Wei[a,c]

[a] School of Environment and Energy, South China University of Technology, Guangzhou 510006, PR China
[b] Guangzhou Key Laboratory for Surface Chemistry of Energy Materials, New Energy Research Institute, Guangzhou 510006, PR China
[c] Guangdong Provincial Key Laboratory of Atmospheric Environment and Pollution Control, Guangzhou 510006, PR China

ARTICLE INFO

Keywords:
Bi_2O_3-TiO_2 Composite
Lead
Dibutyl phthalate
Synergetic photocatalysis

ABSTRACT

A highly efficient Bi_2O_3-TiO_2 composite, prepared by a facile hydrothermal method, can be used for the removal of heavy metal Pb(II) and refractory organic dibutyl phthalate (DBP) from wastewater under visible light irradiation. The photo-induced electrons and holes separately transfer to different locations on the composite, resulting in different photocatalytic reaction sites for the refractory organic oxidation and the heavy metal reduction. This separation in space, thereby greatly improves the photocatalytic efficiency of both reactions. The energy level adjustment caused by Fermi levels matching at the n–p heterojunction, resulted in the Pb(II) being reduced to Pb(0) on the Bi_2O_3-TiO_2 composite in visible light in both the Pb(II)-only and Pb(II)-DBP mixed systems. In contrast, no reduction was observed in visible light using only a Bi_2O_3 or TiO_2 catalyst. Furthermore, the presence of refractory organic DBP in the system significantly increased the removal of Pb(II) while the presence of the more easily degradable phenol increased it to a lesser extent. These results indicate that coupling the reduction rate of heavy metals and the oxidation rate of organics can efficiently enhance the photocatalytic activity of the entire system.

1. Introduction

The multi-factor combined pollution of heavy metals and refractory organics has been a serious environmental problem [1]. Many researchers have reported that heavy metals (Pb, Cr, Cu, Cd, Ni, etc.) and refractory organics (PAHs, EDCs, etc.) mixtures have been detected in oil, coking, electroplating and other industrial wastewater in recent years [2,3]. This discovery has also been found in China's seven major rivers [4,5]. In addition, compared with the single component pollution, these mixtures of pollutants have more severe physiological and biochemical toxic effects on microorganisms, plants and animals than the individual pollutants [6,7].

At present, the heavy metal and refractory organic pollutants in water are mainly treated separately [8–10]. Biological methods, adsorption and advanced oxidation processes, such as O_3 and Fenton oxidations, are commonly used to degrade refractory organics. Precipitation, electrolytic process, activated carbon adsorption, ion exchange and membrane separation can remove heavy metals. Since these methods target different pollutants, which have different molecular structures and physicochemical properties, the processing conditions and equipment are quite different in each case. Thus, it is difficult to satisfy the requirements for simultaneously treating heavy metals and refractory organics in combined wastewater in an effective and economical manner. In short, it would be very helpful to find an effective way to simultaneously remove heavy metals and refractory organics from aqueous systems.

The application of semiconductor photocatalysts, typified by TiO_2, to the task of environmental remediation has attracted considerable attention because of its advantages; e.g., low cost, low toxicity, and stability against photolytic and chemical attack. TiO_2 can generate electrons (e^-) and holes (h^+) under UV light irradiation. On one hand, the h^+ can generate hydroxyl radical (·OH) and hydroperoxyl radical ($\cdot HO_2$) with strong oxidizing properties, which can oxide the organics to CO_2, H_2O or inorganic molecules [11,12]. On the other hand, the e^- can reduce toxic heavy metals, such as Cr(VI) and Cu(II), to low- or non-toxic species [13,14]. Dozzi et al. [15] found that the addition of a dye can promote the reduction of Cr(VI) by TiO_2. Hsu et al. [16] reported that the photocatalytic efficiency of TiO_2 to remove EDTA and Cr(VI) in a mixture of pollutants was much higher than when the pollutants were present separately. However, two major factors limit the application of TiO_2 photocatalysis in environmental decontamination. First, TiO_2 can only be excited by UV light, limiting its application where only visible

* Corresponding author at: School of Environment and Energy, South China University of Technology, Guangzhou 510006, PR China.
E-mail address: huyun@scut.edu.cn (Y. Hu).

https://doi.org/10.1016/j.apcatb.2018.03.025
Received 20 December 2017; Received in revised form 5 March 2018; Accepted 9 March 2018
Available online 10 March 2018
0926-3373/

light is available. Second, the reaction sites of photooxidation and photoreduction are both on the TiO_2 surface, increasing the probability of recombination of the photo-generated electrons and holes.

Research in recent years has addressed these problems by modifying the TiO_2 to facilitate the separation of photoinduced charges through the formation of a heterojunction interface between the two types of semiconductors with matching energy levels [17]. Bi_2O_3 is a narrow gap semiconductor that is excited by visible light. We propose an approach that combines p-type Bi_2O_3 with n-type TiO_2 *in situ* to broaden the light response range and to separate the reaction locations of organic oxidation and heavy metal reduction, thereby resulting in higher efficiency of wastewater treatment of such mixtures.

In general, organic compounds can be photocatalytically oxidized on semiconductors. However, it is the position of the conduction band (CB) of the semiconductor that determines whether the reduction of heavy metals takes place. In the case of the Bi_2O_3-TiO_2 composite catalyst, only Bi_2O_3 can be activated to generate e^- on the CB of Bi_2O_3 by visible light. The CB position determines that the reduction of Cr(VI) (the redox potential of Cr(VI)/Cr(III) is 1.35 eV) can occur, but the reduction of Pb(II) (the redox potential of Pb(II)/Pb is −0.1262 eV) cannot. Additionally, the photocatalytic reduction of Pb(II) is not favored thermodynamically [18]. However, we have found in the present work that Pb(II) is reduced on the synthesized Bi_2O_3-TiO_2 composite, in sharp contrast to the lack of reduction of Pb(II) on Bi_2O_3-only or TiO_2-only under visible light. To the best of our knowledge, there are no researches on the reduction of Pb(II) in a combined system with refractory organics (e.g., PAHs and EDCs) under visible light.

In this work, Bi_2O_3-TiO_2 composites were prepared by a simple hydrothermal method for removal of heavy metal and refractory organic coexisting pollutants under visible light irradiation, using Cr(VI)-DBP and Pb(II)-DBP as model pollutant mixtures. Making full use of photocatalytic oxidation and reduction processes concurrently and separating the reaction sites of these two processes resulted in significantly enhanced photocatalytic performance. Furthermore, the mechanism of the reduction of Pb(II) occurred on the Bi_2O_3-TiO_2 composite under visible light was investigated.

2. Material and methods

2.1. Preparation of the Bi_2O_3-TiO_2 composite photocatalyst

All chemicals used in this study were analytical grade and used without further treatment. In a typical synthesis process, a certain amount of bismuth nitrate pentahydrate was dissolved in a solution of 40 mL of ethanol, 10 mL of deionized water and 2 mL of nitric acid by stirring for 20 min at room temperature and subjecting it to ultrasound for 10 min. The resulting solution was denoted as solution A. In a second mixed solution (B) 10 mL of butyl titanate was added to 10 mL of anhydrous ethanol, and then stirred for 30 min. Subsequently, solutions A and B was mixed together and stirred for another 2 h. Then, the hydrothermal synthesis was carried out in an autoclave at 140 °C for 12 h. After the reaction, precipitates were removed by filtration and washed with deionized water and absolute ethanol, before being dried at 100 °C for 10 h. The molecular composite precursors were then heated to 500 °C at a heating rate of 1 °C/min in a muffle furnace and maintained at that temperature for an additional 4 h. The resulting samples were denoted as x%Bi_2O_3-TiO_2, where x% was the mass ratio of Bi_2O_3 to TiO_2.

2.2. Characterization of Bi_2O_3-Ti_2O_3 catalysts

X-ray diffraction patterns (XRD) of the samples were obtained using a Bruker D8 Advance diffractometer with a Cu Kα radiation (λ = 0.15406 nm) source. Diffraction patterns were obtained over a 2θ range of 10–80° at step intervals of 0.02°. Reflectance measurements were performed on a UV–vis spectrophotometer (Shimadzu, UV-2550) and $BaSO_4$ was used as the reflectance standard. The binding energy was determined by X-ray photoelectron spectroscopy (XPS) with Mg Kα radiation (Axis Ultra DLD). The XPS peaks were calibrated with the C 1s peaks derived from a surface-contaminating hydrocarbon that had a binding energy of 284.4 eV. The ratio of elements was measured with an energy-dispersive spectrometer (EDS) with a dual-detector system (Oxford, X-Max^{N}20). The morphologies and nanostructure of samples were observed by a field-emission scanning electron microscope (FE-SEM, Hitachi, S-4800) and transmission electron microscopy (TEM, JEOL, JEM-2010). High-resolution TEM (HRTEM) was obtained by FEI Tecnai G2 F20 with accelerating voltage of 200 KV. The BET surface area and pore size were measured by Micromeritics ASAP 2020 specific surface area analyzer using nitrogen as absorbent at 77 K.

2.3. Visible light photocatalytic efficiency tests

The photocatalytic experiments were conducted in a custom-constructed reactor. In each case, 1 g/L of catalyst was added to 100 mL of solutions containing 20 mg/L of Cr(VI) or Pb(II) and 5 mg/L of DBP. A 300 W xenon lamp with a light intensity of 100 mW/cm^2 was used as a light source. A UV cut-off filter (λ > 420 nm) removed UV light from the light beam. Before the light was turned on, the solution stood in darkness for 30 min to allow adsorption and desorption equilibration of pollutants on the catalyst. Then the light was switched on. At specified time intervals 10 mL of sample was removed from the reactor and filtered through a 0.45 μm membrane filter.

The concentration of DBP was determined by a high-performance liquid chromatograph (HPLC, Shimadzu LC 20AT), equipped with an HC-C18 (250 × 4.6 mm i. d., 5 μm, Thermo Scientific) column. The mobile phase was a mixture of methanol and water (90:10, V/V), flowing at a rate of 1.0 mL· min^{-1}. The UV detector was operated at 228 nm. The concentration of Cr(VI) was measured by the 1,5-diphenylcarbazide method [19], while the concentration of Pb(II) was determined using a flame atomic absorption spectrometer (AAS).

3. Results and discussion

3.1. Characterization of Bi_2O_3-TiO_2 composites

XRD analysis was used to determine the crystal phase structure and purity of the as-prepared catalyst. The XRD patterns of Bi_2O_3-only, TiO_2-only and x%Bi_2O_3-TiO_2 are shown in Fig. 1(a). These data show that the Bi_2O_3-only catalyst was monoclinic α-Bi_2O_3 (JCPDS NO. 41-1449). The TiO_2-only catalyst has strong diffraction peaks at 2θ = 25.2°, 37.8°, 48°, 53.9°, 55.0°, 62.4° and 68.79°, corresponding to (101), (004), (200), (105), (211), (204) and (116) of anatase TiO_2, respectively (JCPDS NO. 21-1272). After the formation of Bi_2O_3-TiO_2 composite catalysts, the diffraction peaks of the composites were assigned to anatase TiO_2. Note that there were no obvious Bi_2O_3 diffraction peaks observed, which is most likely due to the fact that the Bi_2O_3 in the composite samples were too low or too highly fragmented to present a crystalline diffraction pattern. There was no obvious shift of the diffraction peaks, indicating that the Bi_2O_3 exists as a separate phase rather than being incorporated into the TiO_2 lattice. This behavior is likely, due to the greater size of the Bi atoms (103 pm) compared to the Ti atoms (61 pm) [20]. As the Bi_2O_3 content increases, the intensity of diffraction peaks indicative of TiO_2 gradually weaken, suggesting that the presence of Bi_2O_3 can inhibit the growth of TiO_2 crystals.

UV–Vis analysis was used to study the optical properties of the catalysts. As shown in Fig. 1(b), the absorption edge of TiO_2-only is at about 386.4 nm, while that of Bi_2O_3-only is at about 450.2 nm. According to the absorption photoelectric effect formula, the band gap of Bi_2O_3 and TiO_2 can be calculated to be 2.75 and 3.2 eV, respectively. Compared with TiO_2-only, all composite samples have strong absorption in the visible light range. Specifically, with the increase of Bi_2O_3

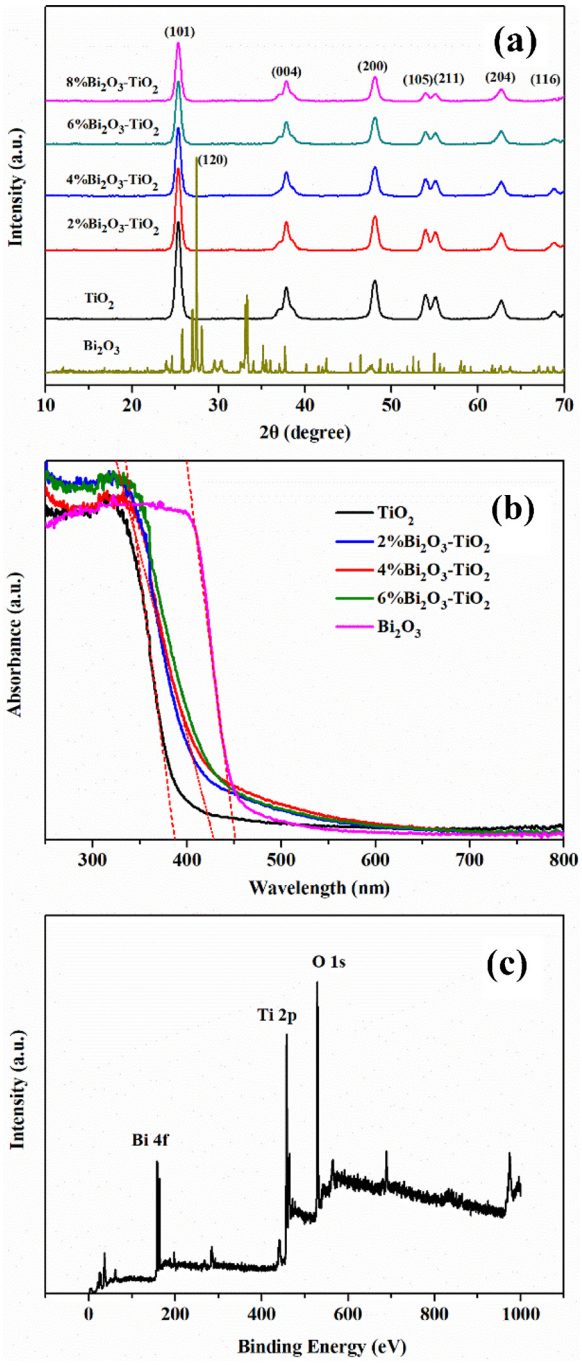

Fig. 1. (a) The XRD patterns and (b) UV–vis diffuse reflection spectra of Bi_2O_3, TiO_2 and x %Bi_2O_3-TiO_2, together with (c) the Survey XPS spectra of 4%Bi_2O_3-TiO_2.

content in the composite, the absorption edge of Bi_2O_3-TiO_2 shifts more towards visible region. These results show that the as-prepared Bi_2O_3-TiO_2 can be excited by visible light. According to the empirical formula calculation [21], the CB and valence band(VB) of TiO_2 are 0.29 and 2.91 eV, and those of Bi_2O_3 are 0.36 and 3.11 eV, respectively (Supporting information).

The surface composition and chemical states of the catalysts were confirmed by XPS analysis, as shown in Figs. 1 and S1. Fig. 1(c) shows the survey spectrum of 4%Bi_2O_3-TiO_2 (where the binding energy for the C 1s peak at 284.6 eV was used as a reference). These data confirm that Bi, O and Ti were present in the composite catalyst and are consistent with the EDS elemental analysis shown in Fig. S2. The C 1s peak in the figure is due to the surface pollution of C. High resolution spectra for Bi 4f and Ti 2p are shown in Figs. S1(a) and (b), respectively. The binding energies at 164.01 and 158.71 eV of Bi_2O_3-only are attributed to Bi $4f_{5/2}$ and Bi $4f_{7/2}$, respectively, which is a feature of Bi^{3+} [22]. In addition, the binding energy at 458.32 and 464.02 eV of TiO_2-only belongs to Ti $2p_{3/2}$ and Ti $2p_{1/2}$, indicating that the main valence state of Ti in the sample is +4 [23]. After Bi_2O_3 composited with TiO_2 (4%Bi_2O_3-TiO_2), the binding energies of Bi 4f and Ti 2p have no obvious shifts, indicating that Bi_2O_3 and TiO_2 exist as separate phases, which is consistent with the XRD result. Fig. S1(c) is an O 1s high resolution spectra. As shown, the O 1s XPS signal is mainly attributed to the contribution of Ti-O in TiO_2 crystal lattice, whose peak position is at 529.42 eV. No obvious peak attributable to the contribution of Bi-O is observed, also demonstrating that the Bi species are not incorporated into the TiO_2 lattice.

The BET surface area of 4%Bi_2O_3-TiO_2 was measured to be 115.89 $m^2 g^{-1}$. The pore size distribution concentrated around 10 nm, as shown in Fig. 2. The morphologies and nanostructures of 4%Bi_2O_3-TiO_2 were shown in Fig. 2, too. The Bi_2O_3 cannot be observed from SEM images directly because of its low content. The HRTEM shows the Bi_2O_3 particles connected closely with the TiO_2 particles.

3.2. Photocatalytic efficiency for the removal of heavy metals and refractory organics

Cr(VI)-DBP and Pb(II)-DBP solutions of mixed pollutants were used to evaluate the performance of the photocatalysts in the reduction of heavy metals and the oxidation of refractory organics. Fig. S3(a) and (b) shows the photocatalytic (visible light ($\lambda > 420$ nm)) activities of Bi_2O_3, TiO_2 and 4%Bi_2O_3-TiO_2 in the removal of Cr(VI) and DBP from their respective single pollutant solutions. The data show that the concentration of Cr(VI) and DBP were unchanged in the absence of catalysts; i.e., "Blank" in Fig. S3(a) and (b). In the presence of Bi_2O_3, the concentrations of the pollutants were only lowered about 2% after 4 h. In the presence of TiO_2, the photocatalytic reduction of Cr(VI) was 14% in 4 h and the photocatalytic oxidation of DBP was 12% in 4 h. When the Bi_2O_3-TiO_2 composite catalyst was used, the removal of Cr(VI) and DBP significantly increased, demonstrating the enhanced photocatalytic activity of Bi_2O_3-TiO_2.

Fig. S4(a) shows the photocatalytic activity of 4%Bi_2O_3-TiO_2 composite in removing Cr(VI) from Cr(VI) only and Cr(VI)-DBP mixed solutions. These data show that the presence of DBP significantly increased the rate and extent of removal of Cr(VI). Likewise, the presence of Cr(VI) significantly increased the rate and extent of removal of DBP (Fig. S4(b)). That is, the photocatalytic efficiency of Bi_2O_3-TiO_2 in the removal of both Cr(VI) and DBP is higher when both pollutants are present together than when only one pollutant is present. When exposed to the Bi_2O_3-TiO_2 composite catalyst, the Cr(VI) captures e^- and is reduced, while the DBP captures h^+ and is oxidized. Under these conditions, the photocatalytic reaction can take full advantage of both oxidation and reduction processes, effectively inhibiting the recombination reaction ($e^- + h^+$), a reaction that does nothing to remove either pollutant.

The effectiveness of Bi_2O_3-TiO_2 composites containing differing amounts of Bi_2O_3 in removing pollutants from Cr(VI)-DBP solutions is shown in Fig. S5. The photocatalytic activity of Bi_2O_3-TiO_2 increased when the Bi_2O_3 content increased from 2% to 4%, presumably due to the broadened spectral response thereby increasing light utilization and the number of separated photo-generated e^- and h^+. Addition of Bi_2O_3 beyond 4% appears to provide additional centers for the recombination of e^- and h^+, thereby lowering the number of reactive agents available for chemically reducing Cr(VI) and oxidizing DBP. Also, at higher concentrations of Bi_2O_3 it is more difficult to achieve uniform mixing in the composite catalyst. Hereafter, we chose 4%Bi_2O_3-TiO_2 as the sample photocatalyst for all the subsequent experiments unless otherwise specified.

The proposed photocatalytic mechanism for the removal of Cr(VI)

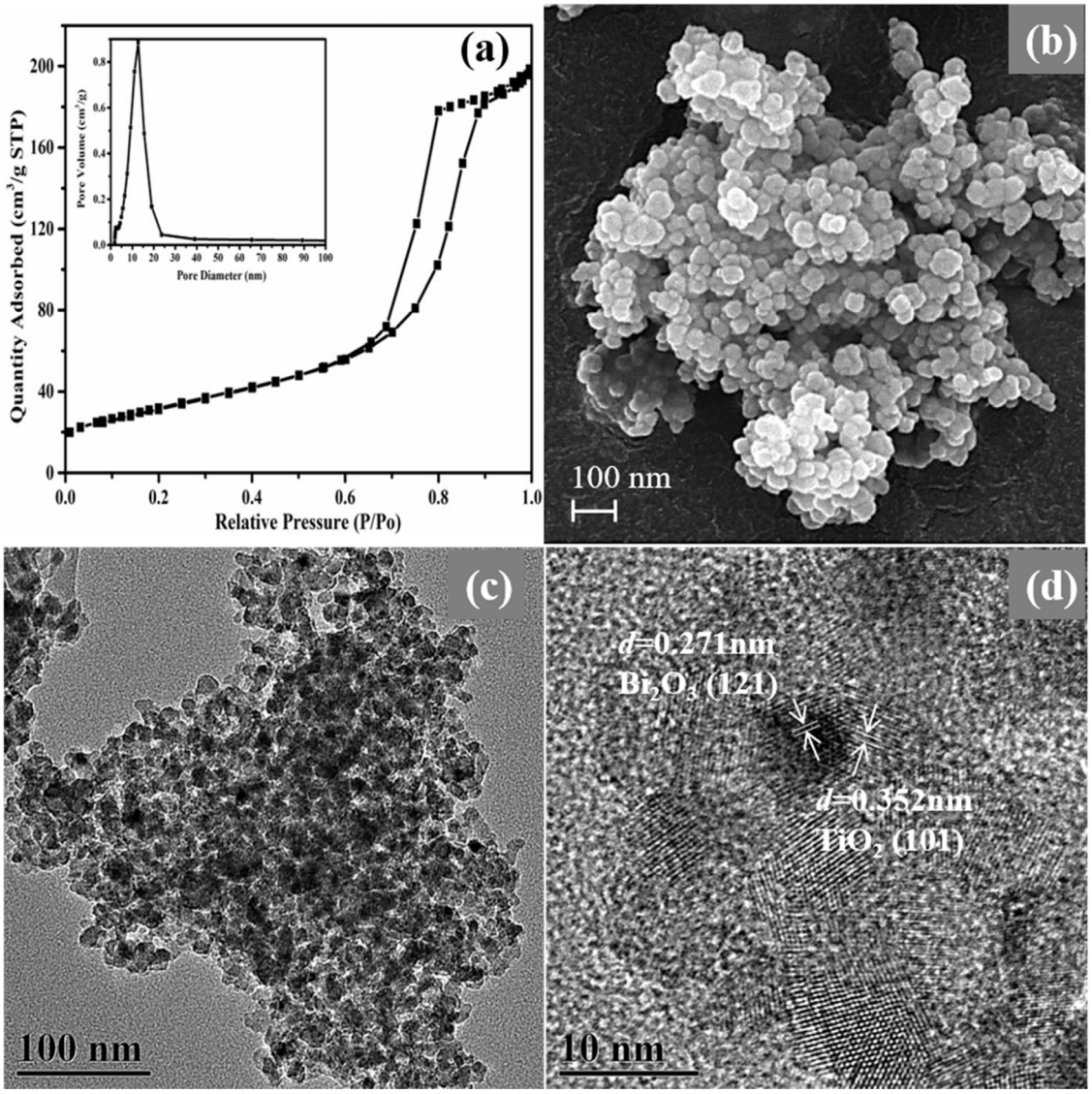

Fig. 2. (a) The N_2 adsorption-desorption isotherms and pore size distribution (b) SEM images (c) TEM and (d) HRTEM images of 4%Bi_2O_3-TiO_2.

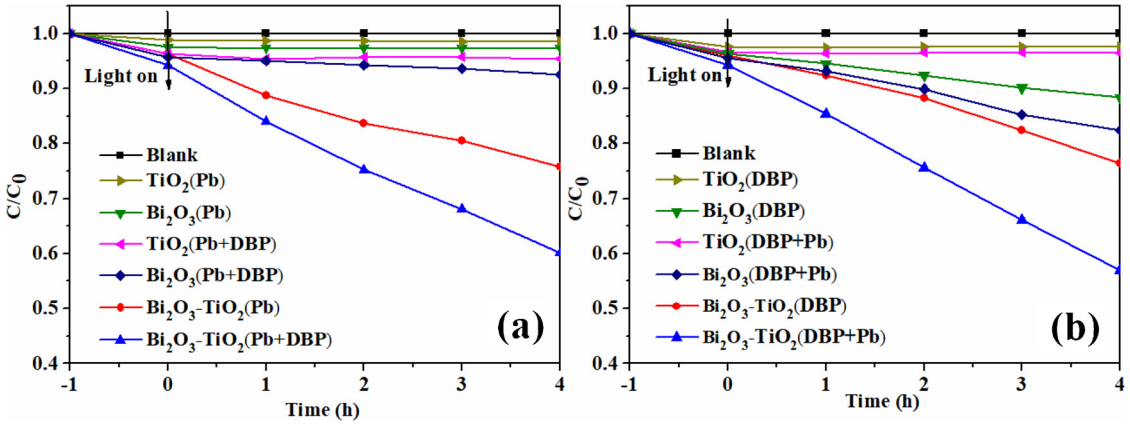

Fig. 3. Photocatalytic activity of Bi_2O_3, TiO_2 and 4%Bi_2O_3-TiO_2 for the removal of Pb(II)-only, DBP-only and Pb(II)-DBP mixed pollutants under visible light irradiation, respectively. Removal of (a) Pb(II) and (b) DBP.

and DBP from the mixed pollutants solution in the presence of Bi_2O_3-TiO_2 is depicted in Scheme S1. Under visible light irradiation, only Bi_2O_3 in the Bi_2O_3-TiO_2 catalyst can be activated. The photo-generated h^+ from the VB of Bi_2O_3 transfers to the VB of TiO_2, where it can further produce ·OH and ·HO_2 radicals that can oxidize DBP into CO_2 and H_2O. The photo-generated e^- can move in the CB of Bi_2O_3 to reduce Cr (VI) to Cr(III). Generally speaking, the more negative the CB position is, the stronger the reducing ability is. However, the CB of Bi_2O_3 is 0.36 eV,

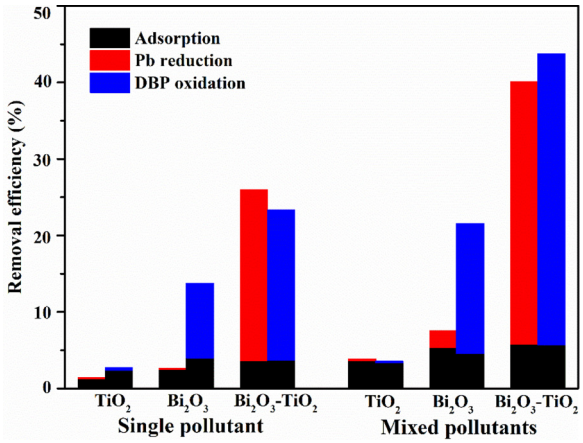

Fig. 4. Photocatalytic efficiency of Bi_2O_3, TiO_2 and 4%Bi_2O_3-TiO_2 for the removal of Pb (II)-only, DBP-only and Pb(II)-DBP mixed pollutants after 4 h of visible light irradiation.

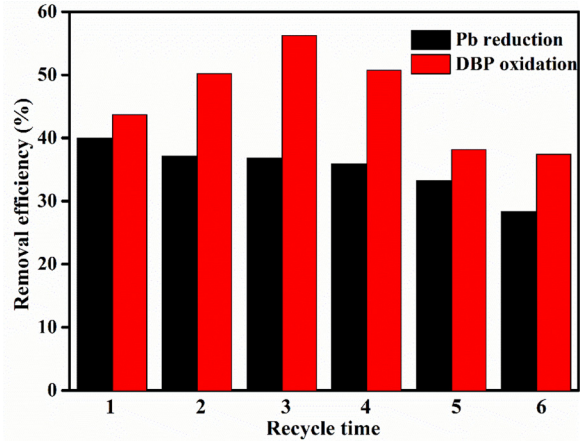

Fig. 5. The recycling photocatalytic activity of 4%Bi_2O_3-TiO_2 composite catalyst for the removal of Pb(II)-DBP mixed pollutants after 4 h of visible light irradiation.

which is more negative than the standard reduction potential of Cr(VI)/Cr(III) (+1.35 eV) but more positive than that of Pb(II)/Pb (−0.1262 eV). Therefore, the reduction of Cr(VI) can occur while that of Pb(II) cannot, as shown in Scheme S1.

As shown in Fig. 3(a), Pb(II) was reduced on the Bi_2O_3-TiO_2 composite catalyst while Pb(II) was not reduced on Bi_2O_3-only or TiO_2-only catalysts under visible light. Furthermore, the presence of DBP significantly increased the removal of Pb ions. At the same time, the presence of Pb(II) promoted the oxidation of DBP on Bi_2O_3-only and Bi_2O_3-TiO_2 catalysts under visible light, as shown in Fig. 3(b). The removal efficiency after 4 h of irradiation on different catalysts was shown in Fig. 4. The Pb reduction only occurred on Bi_2O_3-TiO_2 composite and was enhanced 1.5 times at the presence of DBP compared to Pb(II)-only. The removal efficiency of DBP on Bi_2O_3-TiO_2 composite for the mixed pollutants was nearly 4 times higher than that on Bi_2O_3-only for the single pollutant. All results above suggested that making full use of photocatalytic oxidation and reduction processes concurrently and separating the reaction sites of these two processes can significantly enhance the photocatalytic performance.

For comparing the effects of fabrication methods on photocatalytic activity of Bi_2O_3-TiO_2, the prefabricated anatase TiO_2 and commercial P25 (Degussa) were used to composite with 4%Bi_2O_3. As shown in Fig. S6, both DBP oxidation and Pb(II) reduction efficiency of 4%Bi_2O_3-anatase TiO_2(prefabricated TiO_2) and 4%Bi_2O_3-P25 (Degussa) were worse than that of 4%Bi_2O_3-TiO_2 prepared by one-step fabrication. It indicated that *in-situ* fabrication of Bi_2O_3-TiO_2 can enhance the photocatalytic activities, since closer contact can be more conducive to electrons transformation.

In order to further study the valence change process of Pb ions that accompany their removal from Pb(II)-DBP solutions on Bi_2O_3-TiO_2, the irradiation time was extended. As shown in Fig. S7, after adsorption in the dark for 12 h, the extent of removal of Pb ions was only 8%, and that of DBP was only 6%. After irradiation for 12 h, the concentration of DBP in the solution was close to zero, and there was no detectable Pb(II) after 18 h.

Black particles were found in the solution after irradiation, and the amount of black particles increased with the increased time of irradiation. The black particles were collected for further analysis.

The stability and recyclability of 4%Bi_2O_3-TiO_2 composite were tested by the recycling experiments under visible light irradiation. As shown in Fig. 5, with extended recycling time, the DBP oxidation efficiency increased firstly and decreased after 4 times recycling, while the Pb reduction efficiency decreased gently after 5 times recycling. These results indicated that the depositing species has a limited acceleration effect on DBP oxidation and slight effect on the Pb reduction by contrast.

3.3. The Pb(II) removal process

In order to further explore the removal of Pb(II), XRD and XPS analyses were carried out. Fig. S8 displays the survey XPS spectra of the Bi_2O_3-TiO_2 catalyst before and after dealing with the Pb(II)-DBP mixture solution under visible light. As seen in Fig. S8(b), after adsorption

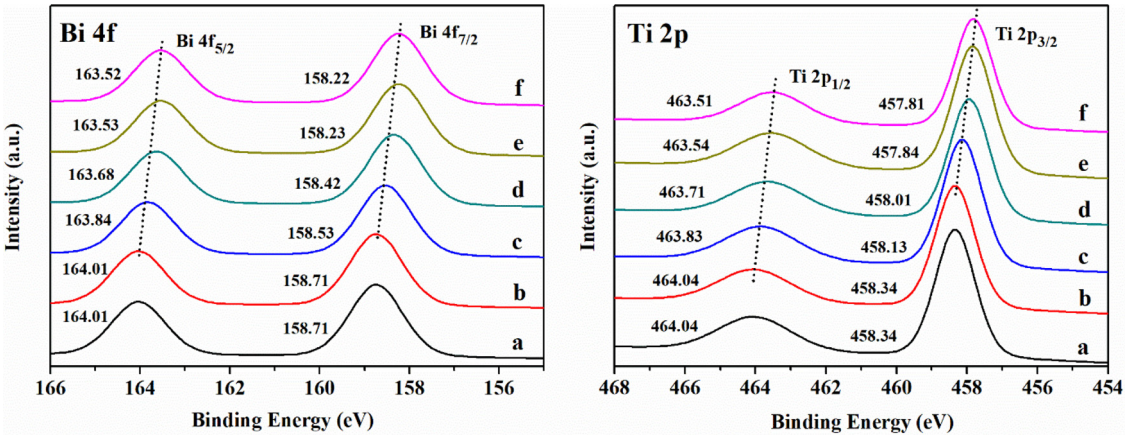

Fig. 6. Bi 4f and Ti 2p high-resolution XPS spectra of 4%Bi_2O_3-TiO_2 composite catalyst before and after dealing with Pb(II)-DBP mixed pollutants under visible light irradiation (a) before the reaction (b) after dark adsorption for 12 h (c) after 4 h of irradiation (d) after for 8 h of irradiation (e) after for 12 h of irradiation (f) after for 18 h of irradiation.

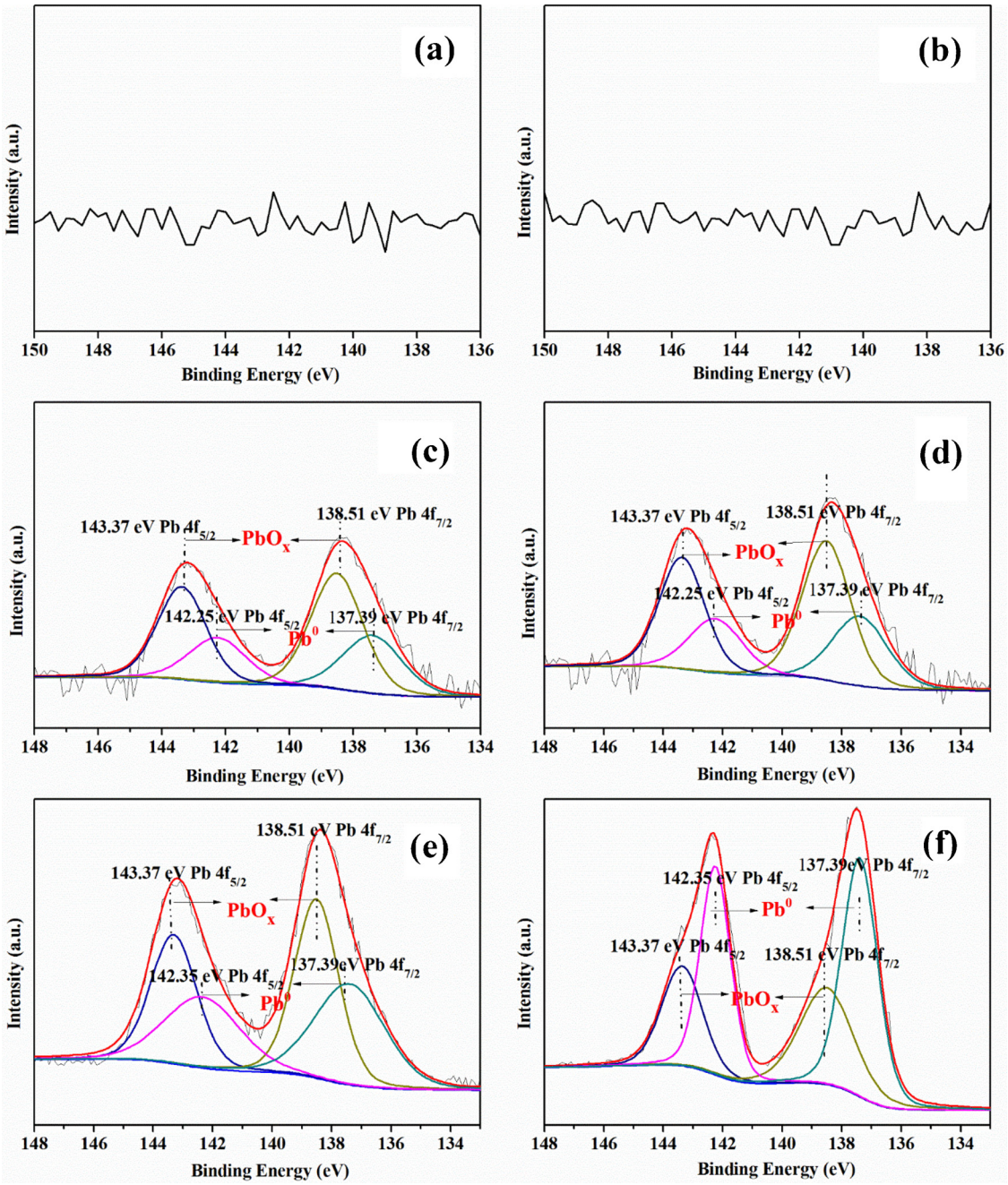

Fig. 7. Pb 4f high-resolution XPS spectra of 4%Bi_2O_3-TiO_2 composite catalyst before and after dealing with Pb(II)-DBP mixed pollutants under visible light radiation (a) before the reaction (b) after dark adsorption for 12 h (c) after 4 h of irradiation (d) after for 8 h of irradiation (e) after for 12 h of irradiation (f) after for 18 h of irradiation.

in the dark for 12 h, there were no peaks belonging to Pb, indicating that adsorption made only a small contribution to the removal of Pb(II). After the light was turned on (Fig. S8(c)–(f)), the peak of Pb gradually increased, indicating that Pb slowly deposited on the surface of catalyst, with a corresponding decrease of the concentration of Pb ions in the solution.

Fig. 6(a) and (b) shows the Bi 4f and Ti 2p high-resolution XPS spectra of Bi_2O_3-TiO_2 before and after dealing with the Pb(II)-DBP mixture. After dark adsorption for 12 h, no obvious shifts were seen. While the binding energies of Bi 4f shifted from 158.71 to 158.22 eV and from 164.01 to 163.52 eV, respectively, and the binding energies of Ti 2p shifted from 458.34 to 457.81 eV and from 464.04 to 463.51 eV, respectively, after irradiation for 18 h. The shifts in the binding energies were probably due to the deposition of Pb particles on the surface of the sample, which led to the changes in the chemical environment surrounding the Bi and Ti atoms.

The Pb 4f high-resolution XPS spectra of the composite Bi_2O_3-TiO_2 catalyst before and after the reaction was shown in Fig. 7. Before and after the dark adsorption for 12 h (Fig. 7(a), (b)), no obvious Pb 4f peak was found, while the Pb 4f peaks appeared after the light was turned on (Fig. 7(c)–(f)). The signals centered at 143.37 and 138.51 eV were assigned to PbO_x, indicating the existence of PbO_x, while those at 142.25 and 137.39 eV were assigned to Pb^0 [24–26]. With the extension of irradiation time, the PbO_x and Pb^0 kept increasing until irradiation for 12 h. After that, the PbO_x started to decrease while the Pb^0 increased after 18 h of irradiation.

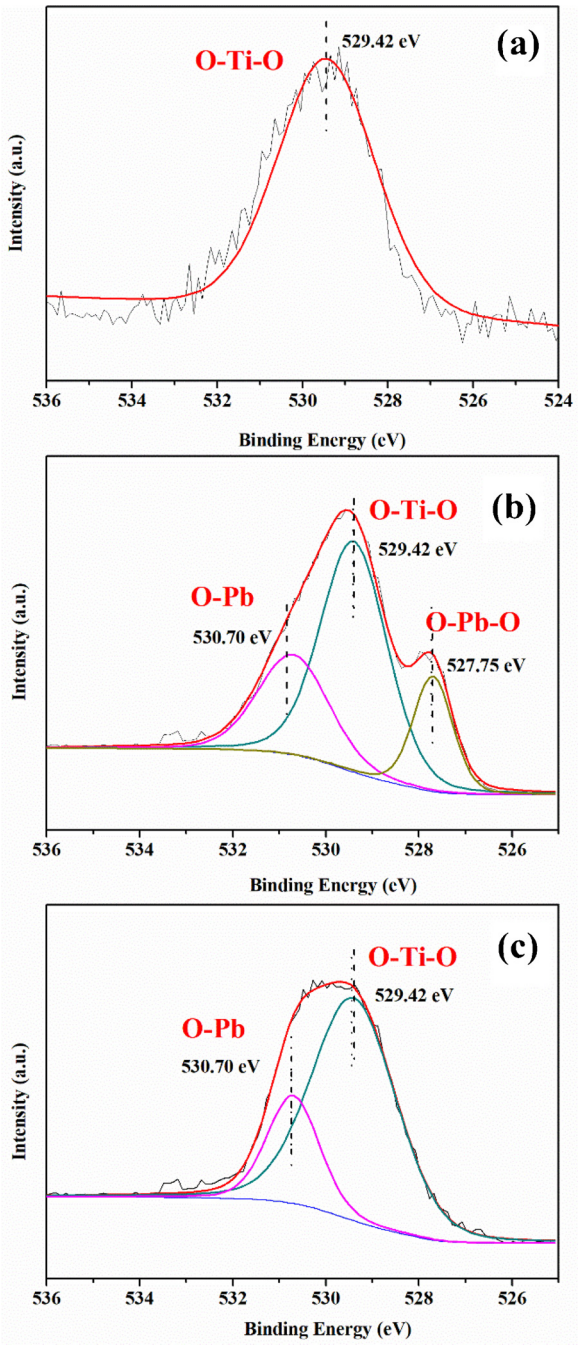

Fig. 8. O 1s high-resolution XPS spectra of 4%Bi_2O_3-TiO_2 composite catalyst before and after dealing with Pb(II)-DBP mixed pollutants under visible light irradiation (a) before the reaction (b) after for 8 h of irradiation (c) after for 18 h of irradiation.

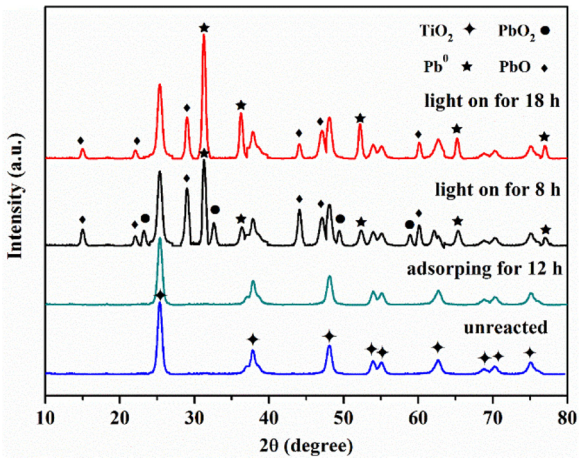

Fig. 9. The XRD patterns of 4%Bi_2O_3-TiO_2 composite catalyst before and after dealing with Pb(II)-DBP mixed pollutants under visible light irradiation.

These results show that at the beginning of the photoreaction, the main chemical states of lead in the reaction products were PbO_x and Pb^0. After irradiation for 12 h, PbO_x started to be reduced to Pb^0 so that the Pb^0 particles soon became the main product.

Also, the O 1s high-resolution XPS spectra of Bi_2O_3-TiO_2 before and after the reaction agreed with the result of Pb 4f (Fig. 8). The signals centered at 530.70 eV were assigned to Pb-O, indicating the existence of PbO, while that at 527.75 eV was assigned to O-Pb-O. After irradiation for 8 h, the peaks of PbO and PbO_2 appeared, while after 18 h, the peak of PbO_2 disappeared and that of PbO decreased, too.

To identify the species deposited on the catalyst, the XRD patterns of Bi_2O_3-TiO_2 before and after dealing with Pb(II)-DBP mixed pollutants were measured. As shown in Fig. 9, all the diffraction peaks were ascribed to anatase TiO_2. Further no obvious Pb peaks were observed after dark adsorption for 12 h, showing that adsorption had little effect on the removal of lead, which was consistent with the result of XPS analyses. After 8 h of the photocatalytic reaction, some new diffraction peaks began to be observed on the catalyst, which were attributed to PbO, Pb^0 and PbO_2, indicating that the initial Pb(II) became PbO, Pb^0 and PbO_2 at points during the irradiation of Pb(II)-DBP on Bi_2O_3-TiO_2. After 18 h of visible light irradiation, the diffraction peak belonging to TiO_2 is still clearly retained, indicating that the as-prepared Bi_2O_3-TiO_2 catalysts were very stable throughout the reactions. However, the diffraction peaks of PbO_2 basically disappeared, and the intensities of the peaks ascribed to PbO diminished. At this point in the experiment, there were no Pb ions remaining in the solution, since all of them and Pb(II) in the solution all turned into Pb^0 and PbO deposited on the catalyst.

Combining the XPS results, a possible sequence of Pb changes is proposed as below:

$$Bi_2O_3 \xrightarrow{h\nu} e^- + h^+ \quad (1)$$

$$Pb^{2+} + 2e^- \rightarrow Pb^0 \quad (2)$$

$$2H_2O + 4h^+ \rightarrow 4H^+ + O_2 \quad (3)$$

$$Pb^{2+} + 2H_2O + 2h^+ \rightarrow PbO_2 + 4H^+ \quad (4)$$

$$2O_2 + 2e^- \rightarrow 2{\bullet}O_2^- \quad (5)$$

$$Pb^{2+} + 2{\bullet}O_2^- \rightarrow PbO_2 + O_2 \quad (6)$$

$$PbO_2 + 2e^- + 2H^+ \rightarrow PbO + H_2O \quad (7)$$

$$PbO + 2e^- + 2H^+ \rightarrow Pb^0 + H_2O \quad (8)$$

In the process of dark adsorption, small amounts of Pb^{2+} and DBP are adsorbed on the Bi_2O_3-TiO_2. After the light is on, the Bi_2O_3-TiO_2 composite catalyst is excited by the visible light and generates electrons and holes (Eq. (1)). Subsequently, some of the adsorbed Pb^{2+} capture e^- and are reduced to form Pb^0 (Eq. (2)), which deposits on the surface of catalyst, while other Pb^{2+} ions capture h^+ and are oxidized to PbO_2 (Eqs. (3), (4)). Furthermore, photo-generated e^- can react with O_2 to generate the superoxide free radical ($\cdot O_2^-$) (Eq. (5)) that can oxidize Pb^{2+} to form PbO_2 (Eq. (6)). However, PbO_2 can be reduced back to PbO by e^- (Eq. (7)), which, in turn, can be further reduced by reaction with e^-, leading to the formation of Pb^0 (Eq. (8)).

In summary, there was evidence of PbO, Pb^0 and PbO_2 simultaneously existing on Bi_2O_3-TiO_2 after irradiation for 8 h. After 18 h, no Pb^{2+} was detected in the solution, and all of the adsorbed PbO_2 particles were reduced to PbO and then reduced further to Pb^0.

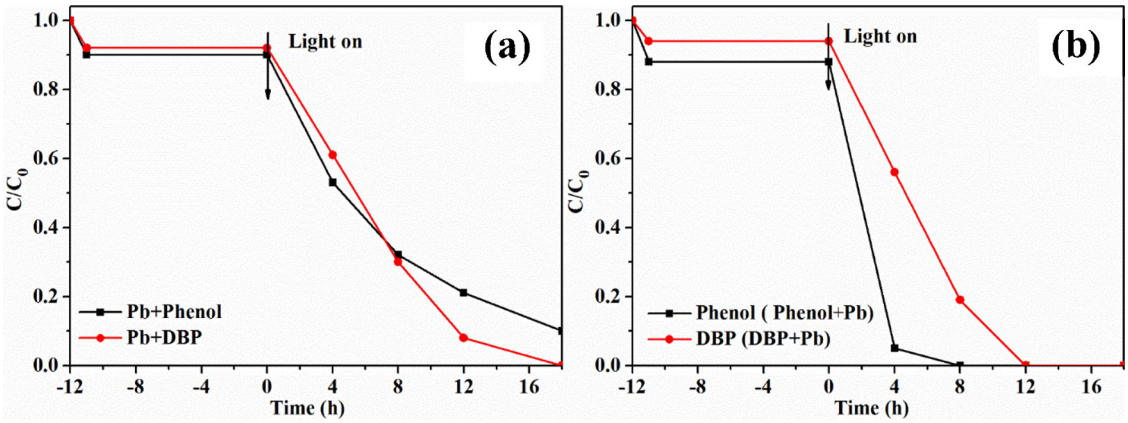

Fig. 10. Photocatalytic activity of 4%Bi_2O_3-TiO_2 dealing with metal-organic mixtures (Pb-phenol and Pb-DBP) under visible light irradiation (a) the variation of Pb^{2+} and (b) organic (phenol and DBP).

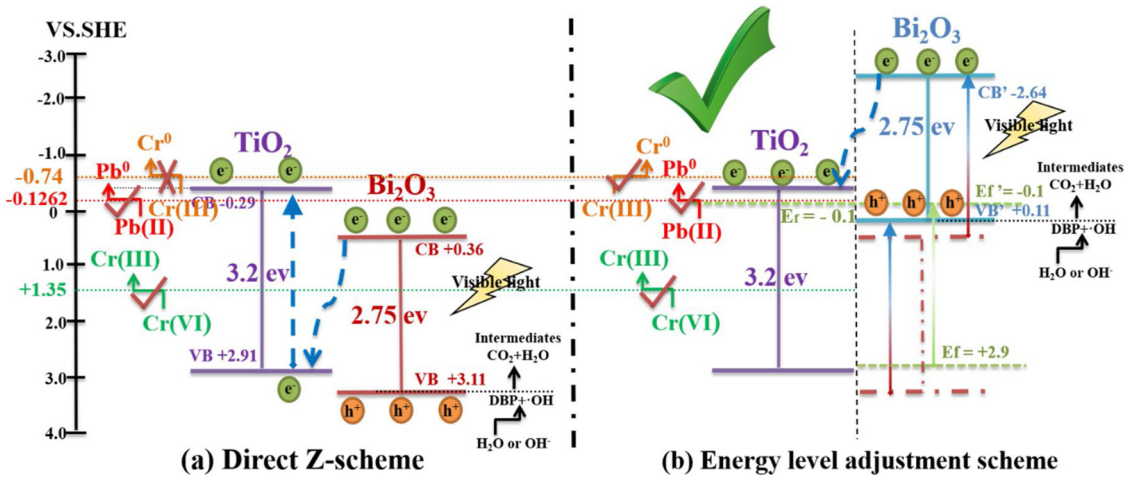

Scheme 1. Synergistic photocatalytic mechanism of the Pb(II)-DBP mixed pollutants removal over Bi_2O_3-TiO_2 composite catalyst under visible light irradiation (a) Direct Z-scheme (b) Energy level adjustment.

3.4. Effect of different organics on the promotion of Pb(II) removal

To investigate the effect of different organics on the removal of Pb (II), phenol, which is more easily oxidized than DBP, was used as a second model substrate. As shown in Fig. 10(a), after visible light irradiation for 4 h, 95% of the phenol had been removed. The phenol oxidation rate was much higher than that of DBP, indicating phenol's greater ability to capture photo-generated holes. As a result, for the first four hours, electrons and holes separated more rapidly in the Pb(II)-phenol solutions than in Pb(II)-DBP solutions, so that the removal rate of Pb ions in the former system was much faster than that the latter (Fig. 10(b)). Eventually, all of the phenol in the solution was oxidized to CO_2 and H_2O and would not be available to serve as hole scavengers. Therefore, the probability of the recombination of photo-generated electrons and holes would increase, resulting in a decrease in the removal efficiency of Pb ions. After visible irradiation for 18 h, there were still some Pb ions in the solution.

In summary, these results indicate that in order to reach optimal photocatalytic performance when using the composite catalyst to treat mixtures of heavy metals and organics, there should be sufficient organic materials available so insure that the oxidation rate of the organics can match the reduction rate of the heavy metals.

3.5. Synergetic photocatalytic mechanism

As mentioned above, for the Bi_2O_3-TiO_2 catalyst, only Bi_2O_3 can be activated by visible light. The CB of Bi_2O_3 is 0.36 eV, which cannot reduce Pb(II). However, the experimental results showed that Pb(II) was actually reduced on Bi_2O_3-TiO_2.

Two major theories can possibly explain this phenomenon according to literature researches [27–34]. The first one is direct Z-scheme [27–31]. When the CB of the activated semiconductor is more positive than that of the proximal semiconductor, the e^- cannot directly transfer to the CB of the proximal semiconductor. However, it can transfer to the VB of the proximal semiconductor firstly. The composite shows stronger reduction abilities because the e^- finally transfers to the CB of the proximal semiconductor. As shown in Scheme 1(a), the e^- transfers from the CB of the visible light activated Bi_2O_3 to the VB of the proximal TiO_2 and finally to the CB of TiO_2. The CB of the composite broadens from +0.36 eV to −0.29 eV, which is more negative than the standard reduction potential of Pb(II)/Pb, and then the Pb(II) reduction occurs. The h^+ at the VB of Bi_2O_3 makes the oxidation of DBP occur.

Another theory is the energy level adjustment scheme [32,34]. When two types of semiconductor materials are in close proximity, the system tends to equilibrium, leading to a uniform Fermi level. A necessary condition is that one must be an n-type semiconductor and another is a p-type. According to the second theory, a possible mechanism for this unexpected Pb(II) photo-reduction on Bi_2O_3-TiO_2 is presented in Scheme 1(b). Specifically, TiO_2 is an n-type semiconductor and Bi_2O_3 is a p-type semiconductor. In general, the flat-band potential of n-type semiconductor is close to its CB potential; i.e., the CB potential is 0.1–0.2 eV more negative than that of its flat-band, while the VB potential of a p-type semiconductor is 0.1–0.2 eV more positive than that of its flat-band [32]. Therefore, the Fermi level in TiO_2 is about

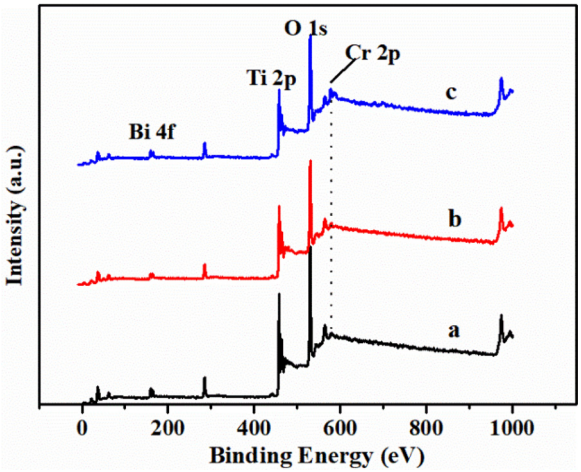

Fig. 11. Survey XPS spectra of 4%Bi_2O_3-TiO_2 composite catalyst before and after dealing with Cr(II)-DBP mixed pollutants under visible light irradiation (a) before the reaction (b) after dark adsorption for 2 h (c) after 4 h of irradiation.

−0.1 eV and that in Bi_2O_3 is about 2.9 eV. Because of the thermodynamic equilibrium, the Fermi level of Bi_2O_3 turns to be same with that of TiO_2 (−0.1 eV) after composition. At this moment, CB and VB of Bi_2O_3 change from +0.36 eV to −2.64 eV and +3.11 eV to +0.11 eV, respectively. As a result, CB potential of Bi_2O_3 is much more negative than the standard reduction potential of Pb(II)/Pb, which makes the reduction of Pb(II) occur.

It seems that two theories both suit for the condition of this experiment. Is it the truth? Another verification was proposed. One of the differences between the two theories is the reduction ability of the composite catalyst. So, we should seek for another metal iron whose standard reduction potential is more negative than the CB of TiO_2 but more positive than the CB of adjusted Bi_2O_3, testing whether the metal iron can be reduced by the Bi_2O_3-TiO_2 composite, and then the question will be answered. The coincidence is that we realize Cr has two reduction potential. One is Cr(VI)/Cr(III), another is Cr(III)/Cr^0. The standard reduction potential of Cr(III)/Cr^0 (−0.74 eV) is just more negative than the CB of TiO_2 (−0.29 eV) and more positive than the CB of adjusted Bi_2O_3 (−2.64 eV).

In order to figure out whether Cr^0 exist, the Bi_2O_3-TiO_2 composite were collected to do the XRD and XPS analyses after dealing with Cr (VI)-DBP mixed pollutants under visible light irradiation. The XRD patterns of 4%Bi_2O_3-TiO_2 composite before and after reaction are shown in Fig. S9. No new peaks or shifts were observed after reaction. Since little change had been made on Bi_2O_3-TiO_2 crystal after reaction, the surface composition and chemical states of the catalysts were confirmed by XPS analysis. The survey XPS spectra of Bi_2O_3-TiO_2 before and after reaction are exhibited in Fig. 11, Cr was present in the composite catalyst after 4 h of irradiation. As shown in Fig. 12, 0.2 eV shift of Bi $4f_{7/2}$ binding energies from 158.71 to 158.51 eV and 0.22 eV shift of Ti $2p_{3/2}$ from 458.34 to 458.12 eV were observed in high-resolution spectra of Bi 4f and Ti 2p, respectively, indicating that the deposition of Cr particles changed the chemical environment surrounding of the Bi and Ti atoms. Fig. 13 shows the Cr 2p high-resolution XPS spectra of the composite Bi_2O_3-TiO_2 catalyst before and after the reaction. Before the dark adsorption (Fig. 13(a)), no obvious Cr 2p peak was found, while the Cr 2p peaks appeared after the dark adsorption for 2 h (Fig. 13(b)). The signals centered at 580.43 and 589.53 eV were assigned to $K_2Cr_2O_7$, indicating the existence of $K_2Cr_2O_7$, while peaks at 578.04 and 587.34 eV were assigned to Cr_2O_3 and those at 576.24 and 585.54 eV were assigned to Cr^0 [35,36]. After 4 h of irradiation, the Cr_2O_3 and Cr^0 appeared (Fig. 13(c)).

These results showed that the Bi_2O_3-TiO_2 catalyst has the ability to reduce Cr(VI) to Cr(III) and then to Cr^0. Thus, the most appropriate mechanism is the energy level adjustment scheme, as shown in Scheme 1(b). Since the energy bands have been adjusted when Bi_2O_3 and TiO_2 are in close proximity, when Bi_2O_3-TiO_2 is irradiated by the visible light, the e^- can transfer from the CB of Bi_2O_3 to the CB of TiO_2, leaving h^+ in the VB of Bi_2O_3. When Bi_2O_3-TiO_2 is exposed to a Pb(II)-DBP mixture, the Pb(II) captures e^- and is reduced on the surface of TiO_2, and the DBP captures the h^+ and is oxidized on the surface of Bi_2O_3, successfully eliminating the recombination of e^- and h^+. The net result is a higher photocatalytic efficiency than exists with the Pb(II)-only or DBP-only solutions. Moreover, the reduction of heavy metals and oxidation of organics occur on different surface sites of the composite semiconductor, reducing the competition between the two kinds of pollutants for the same active site, thereby further contributing to enhanced catalytic performance.

4. Conclusions

In this work, the synthesized Bi_2O_3-TiO_2 composite catalyst improved the photocatalytic efficiency of simultaneously removing both heavy metals and refractory organics from wastewater under visible light irradiation. Making full use of photocatalytic oxidation and reduction processes concurrently and separating the reaction sites of these two processes resulted in significantly enhanced photocatalytic performance. Both Cr-DBP and Pb-DBP mixtures were successfully treated by Bi_2O_3-TiO_2 composite catalysts under visible light. The reduction of Pb(II)/Pb^0 and Cr(III)/Cr^0 occurred on the Bi_2O_3-TiO_2 composite under visible light because of the energy level adjustments

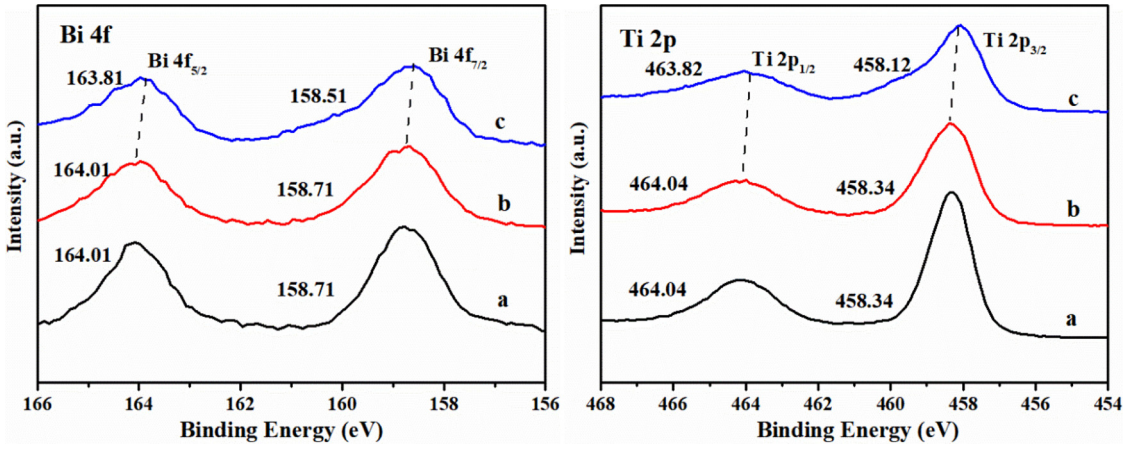

Fig. 12. Bi 4f and Ti 2p high-resolution XPS spectra of 4%Bi_2O_3-TiO_2 composite catalyst before and after dealing with Cr(VI)-DBP mixed pollutants under visible light irradiation (a) before the reaction (b) after dark adsorption for 2 h (c) after 4 h of irradiation.

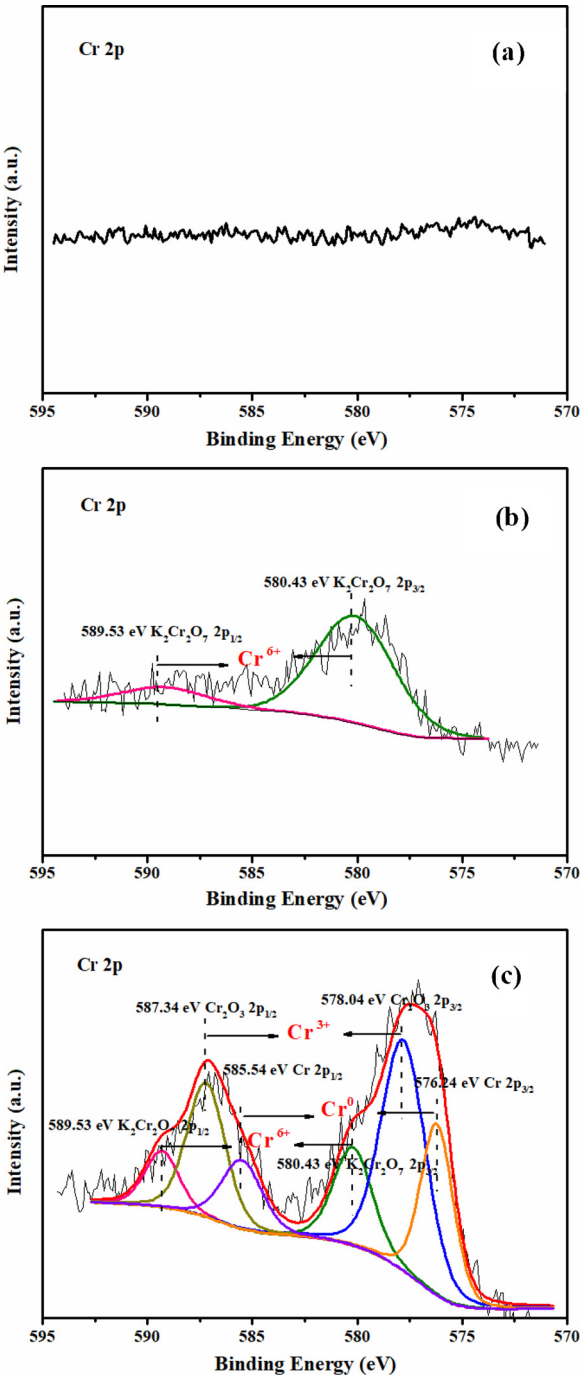

Fig. 13. Cr 2p high-resolution XPS spectra of 4%Bi_2O_3-TiO_2 composite catalyst before and after dealing with Cr(VI)-DBP mixed pollutants under visible light irradiation (a) before the reaction (b) after dark adsorption for 2 h (c) after 4 h of irradiation.

that were caused by Fermi level matching at the n–p heterojunctions. In order to achieve optimal photocatalytic performance, the oxidation rate of organics should match the reduction rate of heavy metals. This work provides a new strategy for the application of visible-light-driven photocatalysts in treating heavy metal-organic mixed wastewater.

Acknowledgments

This work was supported by National Natural Science Foundation of China (21577039, 21777047, 21277051), Science and Technology Planning Project of Guangdong Province, China (2015A020215004) and Scientific Research Project of Guangzhou City (201804020026). We are grateful to Dr. Donald G. Barnes for providing helpful advice to our paper.

Appendix A. Supplementary data

Supplementary material related to this article can be found, in the online version, at doi:https://doi.org/10.1016/j.apcatb.2018.03.025.

References

[1] X. Weng, S. Lin, Y. Zhong, Z. Chen, Chitosan stabilized bimetallic Fe/Ni nanoparticles used to remove mixed contaminants-amoxicillin and Cd(II) from aqueous solutions, Chem. Eng. J. 229 (2013) 27–34.
[2] J. Shim, J. Lim, P. Shea, B. Oh, Simultaneous removal of phenol, Cu and Cd from water with corn cob silica-alginate beads, J. Hazard. Mater. 272 (2014) 129–136.
[3] P. Burmistrz, A. Rozwadowski, M. Burmistrz, A. Karcz, Coke dust enhances coke plant wastewater treatment, Chemosphere 117 (2014) 278–284.
[4] J. Feng, M. Zhai, J. Sun, Q. Liu, Distribution and sources of polycyclic aromatic hydrocarbons (PAHs) in sediment from the upper reach of Huaihe River, East China, Environ. Sci. Pollut. Res. 19 (2012) 1097–1106.
[5] Q. Gao, Y. Li, Q. Cheng, M. Yu, B. Hu, Z. Wang, Z. Yu, Analysis and assessment of the nutrients, biochemical indexes and heavy metals in the Three Gorges Reservoir, China, from 2008 to 2013, Water Res. 92 (2016) 262–274.
[6] J. Zhu, Z. Zhao, Y. Lu, Evaluation of genotoxicity of combined soil pollution by cadmium and phenanthrene on earthworm, J. Environ. Sci. 18 (2006) 1210–1215.
[7] M. Vohra, A. Davis, TiO_2-assisted photocatalysis of lead–EDTA, Water Res. 34 (2000) 952–964.
[8] J. Sumpter, A. Johnson, Lessons from endocrine disruption and their application to other issues concerning trace organics in the aquatic environment, Environ. Sci. Technol. 39 (2005) 4321–4332.
[9] G. Zhao, J. Li, X. Ren, C. Chen, X. Wang, Few-layered graphene oxide nanosheets as superior sorbents for heavy metal ion pollution management, Environ. Sci. Technol. 45 (2011) 10454–10462.
[10] Y. Ren, K. Nakano, M. Nomura, N. Chiba, O. Nishimura, Effects of bacterial activity on estrogen removal in nitrifying activated sludge, Water Res. 41 (2007) 3089–3096.
[11] M. Nalbandian, K. Greenstein, D. Shuai, M. Zhang, Y. Choa, G. Parkin, D. Cwiertny, Tailored synthesis of photoactive TiO_2 nanofibers and Au/TiO_2 nanofiber composites: structure and reactivity optimization for water treatment applications, Environ. Sci. Technol. 49 (2015) 1654–1663.
[12] J. Wang, P. Zhang, X. Li, J. Zhu, H. Li, Synchronical pollutant degradation and H_2 production on a Ti^{3+}-doped TiO_2 visible photocatalyst with dominant (001) facets, Appl. Catal. B: Environ. 134 (2013) 198–204.
[13] X. Pan, Z. Yi, Graphene oxide regulated tin oxide nanostructures: engineering composition, morphology, band structure, and photocatalytic properties, ACS Appl. Mater. Interfaces 7 (2015) 27167–27175.
[14] A. Giannakas, M. Antonopoulou, J. Papavasiliou, Y. Deligiannakis, I. Konstantinou, Photocatalytic performance of Pt-TiO_2, Pt-N-TiO_2 and Pt-N/F-TiO_2 towards simultaneous Cr(VI) reduction/benzoic acid oxidation: Insights into photogenerated charge carrier dynamics and catalyst properties, J. Photochem. Photobiol. A: Chem. 349 (2017) 25–35.
[15] M. Dozzi, A. Saccomanni, E. Selli, Cr(VI) photocatalytic reduction: effects of simultaneous organics oxidation and of gold nanoparticles photodeposition on TiO_2, J. Hazard. Mater. 211 (2012) 188–195.
[16] H. Hsu, S. Chen, Y. Tang, H. Hsi, Enhanced photocatalytic activity of chromium (VI) reduction and EDTA oxidization by photoelectrocatalysis combining cationic exchange membrane processes, J. Hazard. Mater. 248 (2013) 97–106.
[17] G. Li, Z. Lian, W. Wang, D. Zhang, H. Li, Nanotube-confinement induced size-controllable g-C_3N_4quantum dots modified single-crystalline TiO_2 nanotube arrays for stable synergetic photoelectrocatalysis, Nano Energy 19 (2016) 446–454.
[18] S. Park, S. Kim, G.J. Sun, C. Lee, Synthesis, structure, and ethanol gas sensing properties of In_2O_3 nanorods decorated with Bi_2O_3 nanoparticles, ACS Appl. Mater. Interfaces 7 (2015) 8138–8146.
[19] X. Pan, Z. Yi, Graphene oxide regulated tin oxide nanostructures: engineering composition, morphology, band structure, and photocatalytic properties, ACS Appl. Mater. Interfaces 7 (2015) 27167–27175.
[20] J. Xu, Y. Ao, D. Fu, C. Yuan, Synthesis of Bi_2O_3-TiO_2 composite film with high-photocatalytic activity under sunlight irradiation, Appl. Surf. Sci. 255 (2008) 2365–2369.
[21] J. Zhu, S. Wang, J. Wang, D. Zhang, H. Li, Highly active and durable Bi_2O_3/TiO_2 visible photocatalyst in flower-like spheres with surface-enriched Bi_2O_3 quantum dots, Appl. Catal. B: Environ. 102 (2011) 120–125.
[22] W. Shan, Y. Hu, Z. Bai, M. Zheng, C. Wei, In situ preparation of g-C_3N_4/bismuth-based oxide nanocomposites with enhanced photocatalytic activity, Appl. Catal. B: Environ. 188 (2016) 1–12.
[23] X. Song, Y. Hu, M. Zheng, C. Wei, Solvent-free in situ synthesis of g-C_3N_4/{001}TiO_2 composite with enhanced UV-and visible-light photocatalytic activity for NO oxidation, Appl. Catal. B: Environ. 182 (2016) 587–597.
[24] K. Kim, T. O'leary, N. Winograd, X-ray photoelectron spectra of lead oxides, Anal. Chem. 45 (1973) 2214–2218.
[25] H. Kanai, M. Yoshiki, M. Hayashi, R. Kuwae, Y. Yamashita, Grain-boundary-phase identification of a lead-based relaxor by X-ray photoelectron spectroscopy, J. Am. Ceram. Soc. 77 (1994) 2229–2231.

[26] Z. He, Y. Qi, J. Yu, R. Chi, Modified sugarcane bagasse for adsorption of Pb(2+) and Cd(2+), Environ. Sci. Technol. 10 (2012) 58–61.
[27] J. Yu, S. Wang, J. Low, W. Xiao, Enhanced photocatalytic performance of direct Z-scheme g-C_3N_4-TiO_2 photocatalysts for the decomposition of formaldehyde in air, Phys. Chem. Chem. Phys. 15 (2013) 16883–16890.
[28] K. Wang, G. Zhang, J. Li, Y. Li, X. Wu, 0D/2D Z-scheme heterojunctions of bismuth tantalite quantum dots/ultrathin g-C_3N_4 nanosheets for highly efficient visible light photocatalytic degradation of antibiotics, ACS Appl. Mater. Interfaces (2017) 43704–43715.
[29] K. Qi, B. Cheng, J. Yu, W. Ho, A review on TiO_2-based Z-scheme photocatalysts, Chin. J. Catal. 38 (2017) 1936–1955.
[30] J. Low, C. Jiang, B. Cheng, S. Wageh, A. Al-Ghamdi, J. Yu, A review of direct Z-scheme photocatalysts, Small Methods 1 (2017) 1700080.
[31] J. Low, J. Yu, M. Jaroniec, S. Wageh, A. Al-Ghamdi, Heterojunction photocatalysts, Adv. Mater. 29 (2017) 1601694.
[32] S. Morrison, Electrochemistry at Semiconductor and Oxidized Metal Electrodes, Plenum Press, New York, London, 1980.
[33] Y. Hu, D. Li, Y. Zheng, W. Chen, Y. He, Y. Shao, X. Fu, G. Xiao, $BiVO_4$/TiO_2 nanocrystalline heterostructure: a wide spectrum responsive photocatalyst towards the highly efficient decomposition of gaseous benzene, Appl. Catal. B: Environ. 104 (2011) 30–36.
[34] L. Yang, S. Luo, Y. Li, Y. Xiao, Q. Kang, Q. Cai, High efficient photocatalytic degradation of p-nitrophenol on a unique Cu_2O/TiO_2 pn heterojunction network catalyst, Environ. Sci. Technol. 44 (2010) 7641–7646.
[35] Z. Wu, X. Yuan, G. Zeng, L. Jiang, H. Zhong, Y. Xie, H. Wang, X. Chen, H. Wang, Highly efficient photocatalytic activity and mechanism of Yb^{3+}/Tm^{3+}codoped In_2S_3 from ultraviolet toear infrared light towards chromium (VI) reduction and rhodamine B oxydative degradation, Appl. Catal. B: Environ. 225 (2018) 8–21.
[36] H. Wang, X. Yuan, Y. Wu, X. Chen, L. Leng, H. Wang, G. Zeng, Facile synthesis of polypyrrole decorated reduced graphene oxide–Fe_3O_4 magnetic composites and its application for the Cr (VI) removal, Chem. Eng. J. 262 (2015) 597–606.